ADVANCED FUNCTIONAL MATERIALS
www.afm-journal.de

Materials Views
www.MaterialsViews.com

Synthesis, Structure Transformation, and Electrochemical Properties of Li_2MgSi as a Novel Anode for Li-Ion Batteries

*Yongfeng Liu, Ruijun Ma, Yanping He, Mingxia Gao, and Hongge Pan**

In this work, a novel hexagonal Li_2MgSi anode is successfully prepared through a hydrogen-driven chemical reaction technique. Electrochemical tests indicate significantly improved cycling stability for the as-synthesized Li_2MgSi compared with that of Mg_2Si. Ball-milling treatment induces a polymorphic transformation of Li_2MgSi from a hexagonal structure to a cubic structure, suggesting that the cubic Li_2MgSi is a metastable phase. The post-24-h-milled Li_2MgSi delivers a maximum capacity of 807.8 mAh g^{-1}, which is much higher than that of pristine Li_2MgSi. In particular, the post-24-h-milled Li_2MgSi retains 50% of its capacity after 100 cycles, which is superior to cycling stability of Mg_2Si. XRD analyses correlated with CV measurements do not demonstrate the dissociation of metallic Mg and/or Li–Mg alloy involved in the lithiation of Mg_2Si for the Li_2MgSi anode, which contributes to the improved lithium storage performance of the Li_2MgSi anode. The findings presented in this work are very useful for the design and synthesis of novel intermetallic compounds for lithium storage as anode materials of Li-ion batteries.

1. Introduction

Li-ion batteries (LIBs) with high energy densities and high power performances are the technology of choice for future hybrid electric vehicles and renewable energy storage.[1–4] However, current commercialized graphite anodes have a low capacity (372 mAh g^{-1}) and poor rate capability, which cannot meet the demand of high-performance battery systems.[5] Intermetallic compounds have attracted intensive interest as promising candidate anodes due to their high capacities.[6–11] One example is magnesium silicide (Mg_2Si), which possesses a highly specific capacity of 1370 mAh g^{-1}, corresponding to 3.9 Li per Mg_2Si, and exhibits a favorable voltage profile. In addition, the constituent elements of Mg and Si are naturally abundant and inexpensive.[12,13]

Unfortunately, Mg_2Si electrodes show rapid capacity fading, which prevents their use in practical applications. The electrical isolation of the active materials caused by the expansion/contraction is believed to be the most important reason for this degradation in capacity.[13] Therefore, considerable efforts have been devoted to preparing thin-film electrodes and Mg_2Si/C composites for improving the electrochemical performance of Mg_2Si anodes.[12,14] However, it has been observed that the diffraction peaks of Mg emerge in the corresponding XRD profile after the first delithiation process and then accumulate upon cycling. This phenomenon suggests that the regeneration reaction of Mg_2Si during delithiation is not thoroughly completed.[15] It has also been reported that during lithiation, the insertion of Li into Mg_2Si occurs first, and Li_2MgSi with a cubic fluorite-type structure is then formed along with the extraction of Mg from Mg_2Si. Lastly, Li_2MgSi is converted to Li–Mg and Li–Si alloys at low current densities and low potentials.[15,16] Therefore, the irreversible formation of metallic Mg and/or Li–Mg alloy should also be responsible for the capacity degradation of Mg_2Si upon cycling. Further electronic energy calculations regarding Li-intercalated Mg_2Si and the formation of Li_2MgSi have revealed that retarding the generation of metallic Mg would lead to an improvement in the reversibility of lithium insertion/extraction into/from Mg_2Si.[17] One proposed method is to directly use Li_2MgSi as an anode material, which can prevent the dissociation of metallic Mg and/or Li–Mg alloy from Mg_2Si. Moreover, the pre-lithiated Li_2MgSi is likely to reduce the stress/strain during delithiation/lithiation, which is also favorable for improving the cycling performance of the electrodes. However, no attempt has been made to determine the electrochemical properties of Li_2MgSi as an anode material to date because it is rather difficult to prepare high-purity Li_2MgSi by conventional melting techniques due to the large discrepancies between the melting points of Si (1410 °C), Mg (649 °C), and Li (180 °C).

Recently, we proposed a novel hydrogen-driven chemical reaction (HDCR) method to prepare Li–Si and Mg–Si alloys.[18,19] By replacing the alkali and alkaline earth metals with the corresponding hydrides, the large difference in the melting points of Si and the alkali/alkaline earth metals can be avoided, and Mg_2Si and $Li_{12}Si_7$ alloys with high purity have been successfully obtained. Herein, the newly developed HDCR technique was employed to synthesize Li_2MgSi. The results show that a novel hexagonal Li_2MgSi anode can be successfully synthesized using the HDCR technique. The lithium insertion/extraction

Prof. Y. F. Liu, Dr. R. J. Ma, Y. P. He,
Prof. M. X. Gao, Prof. H. G. Pan
State Key Laboratory of Silicon Materials
Key Laboratory of Advanced Materials
and Applications for Batteries of Zhejiang Province
Department of Materials Science and Engineering
Zhejiang University
Hangzhou 310027, People's Republic of China
E-mail: hgpan@zju.edu.cn

DOI: 10.1002/adfm.201304287

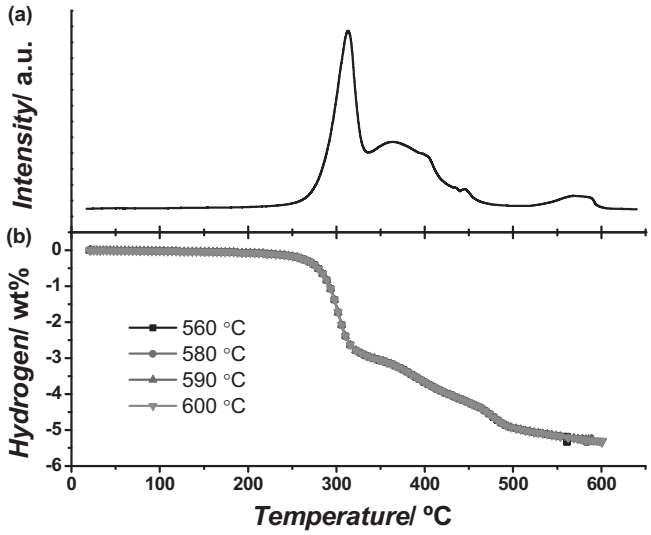

Figure 1. a) TPD curve and b) dehydrogenation curves of the 2LiH-MgH_2-Si sample.

behaviors of the as-prepared Li_2MgSi anode materials were investigated. Interestingly, a polymorphic transformation from the hexagonal structure to the cubic structure was observed for Li_2MgSi after 2 h of ball milling. Moreover, the effects of ball-milling duration on the particle sizes and electrochemical properties of the Li_2MgSi electrodes were systematically elucidated, and the lithium-storage mechanisms of the cubic Li_2MgSi electrodes were also discussed. Our findings are very useful for the design and synthesis of novel intermetallic compounds for lithium storage as anode materials of Li-ion batteries.

2. Results and Discussion

2.1. Preparation of Li_2MgSi

To determine an appropriate reaction temperature for the preparation of Li_2MgSi, the qualitative dehydrogenation behavior of the 2LiH-MgH_2-Si sample was first examined by TPD. **Figure 1**a shows the TPD curve of the 2LiH-MgH_2-Si sample. The results show that more than three dehydrogenation peaks occurred in the TPD profile as the as-milled 2LiH-MgH_2-Si mixture was heated from room temperature to 640 °C, indicating multistep dehydrogenation behavior. Hydrogen release from the 2LiH-MgH_2-Si mixture begins sluggishly at ≈150 °C and terminates at ≈600 °C. Figure 1b presents the dehydrogenation curves of the samples heated to 560, 580, 590, and 600 °C, respectively. For comparison, the dehydrogenation amount was further plotted as a function of heating time (see Figure S1, Supporting Information). It can be observed that a total of ≈5.34 wt% hydrogen was released for the as-prepared 2LiH-MgH_2-Si mixture even at 560 °C. This value is quite close to the theoretical hydrogen content in the 2LiH-MgH_2-Si mixture (5.73 wt%), suggesting that the dehydrogenation reaction was completed.

Figure 2 shows the XRD patterns of 2LiH-MgH_2-Si samples before and after dehydrogenation. The characteristic reflections of LiH, MgH_2 and Si were detected without additional peaks in the XRD profile of the as-milled mixture, indicating that the mixture mainly consisted of the three starting chemicals. That is, the as-milled 2LiH-MgH_2-Si sample was only a physical mixture of LiH, MgH_2 and Si. After thermal dehydrogenation at 560 °C, a new set of peaks dominated the XRD pattern along with the disappearance of the peaks of LiH, MgH_2, and Si, revealing the formation of a new species. Moreover, the Mg_2Si phase was also identified from the diffraction peaks at 2θ values of 24.0°, 47.3°, 58.0°, and 72.4°, although their intensities were rather weak. As the dehydrogenation temperature was increased to 580 and 590 °C, only the newly developed peaks were discernible and the characteristic peaks of Mg_2Si disappeared. Because only hydrogen was removed from the mixture upon heating, the composition of the resulting solid-state product should be Li_2MgSi. Further EDS analyses confirmed that the Mg/Si atomic ratio was nearly 1:1 (see Figure S2, Supporting Information). Therefore, the chemical reaction process can be described as follows while heating the 2LiH-MgH_2-Si mixture to 590 °C:

$$MgH_2 + 2LiH + Si \rightarrow Li_2MgSi + 2H_2 \quad (1)$$

However, upon further elevating the reaction temperature to 600 °C, the typical diffraction peaks of Mg_2Si reappeared with considerable intensities. At the same time, an additional Li_4Si alloy phase was also observed, although Li_2MgSi remained the primary phase in the XRD profile of the

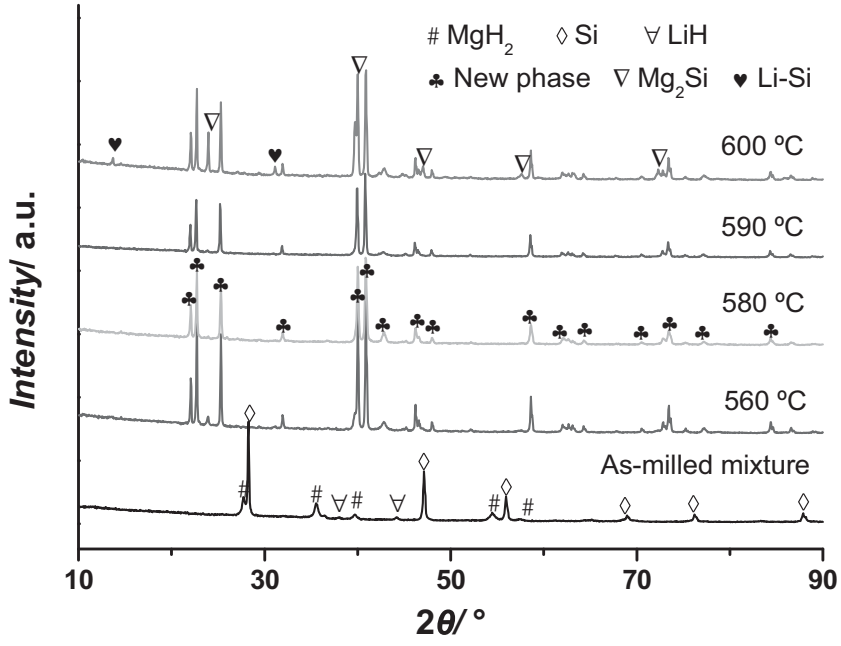

Figure 2. XRD patterns of 2LiH-MgH_2-Si samples before and after dehydrogenation at different temperatures. #: MgH_2, ◊: Si, ∀: LiH, ♣: new phase, ∇: Mg_2Si, ♥: Li-Si.

solid-state product. These results suggest that higher reaction temperatures lead to the phase separation of Li_2MgSi to yield Mg_2Si and Li_4Si. Moreover, SEM images show some agglomerated and grown particles at a dehydrogenation temperature above 580 °C (see Figure S3, Supporting Information). As a result, the reaction temperature for the formation of Li_2MgSi by heating the 2LiH-MgH_2-Si mixture was optimized to be 580 °C.

In addition, it is noteworthy that the new XRD pattern observed in Figure 2 can be indexed to a hexagonal cell with lattice parameters of $a = b = 4.510$ Å, $c = 8.021$ Å, and $V = 141.3$ Å^3. This pattern is distinctly different from that previously reported for the Li_2MgSi phase.[20–22] Roberts et al. synthesized Li_2MgSi by ball milling Mg powder, Si powder and Li granules and revealed that the final material possessed a cubic $Fm\bar{3}m$ structure,[15] which is very similar to that formed in situ during Li insertion into Mg_2Si.[21] In this case, however, Li_2MgSi was prepared by heating a 2LiH-MgH_2-Si mixture. The different treatment processes employed possibly contributed to the various crystal structures that were obtained. We therefore believe that Li_2MgSi should be a polymorphic material.

2.2. Electrochemical Lithium Storage Properties of Hexagonal Li_2MgSi

The as-prepared hexagonal Li_2MgSi was used as an anodic active material, and half-cells were assembled to evaluate its electrochemical lithium-storage properties. The half-cells were cycled at a constant current density of 100 mA g^{-1} between 0.01 and 3.0 V (vs Li/Li$^+$). To reduce the possibly existed Si_xO and MgO and form a stable solid electrolyte interface (SEI) film on the surface, the as-prepared Li_2MgSi was first lithiated in the first cycle. **Figure 3**a shows the galvanostatic charge/discharge voltage profiles of the as-prepared hexagonal Li_2MgSi. It is observed that approximately 286 mAh g^{-1} of capacity was discharged in the first discharge, indicating that more Li was inserted into Li_2MgSi. According to a previous report, the Li_2MgSi intermediate is further lithiated to form Li–Mg and Li–Si alloys at lower potentials during the lithiation of Mg_2Si.[15] Interestingly, the first charge capacity was approximately 597 mAh g^{-1}, distinctly higher than the first discharge capacity. The corresponding Coulombic efficiency was calculated to be 208.8%, much higher than 100%. This finding suggests that the chemically pre-inserted Li can be electrochemically extracted reversibly during the charge process. After the first discharge/charge cycle, a maximum discharge capacity of 649.9 mAh g^{-1} was reached, and the corresponding charge capacity was 614.2 mAh g^{-1} with a rather high Coulombic efficiency of ≈94.5% (Figure 3b). The Coulombic efficiency rapidly increased to 98% within three cycles. For the Mg_2Si electrode, the first discharge capacity was as high as ≈1095 mAh g^{-1}, whereas the corresponding Coulombic efficiency was determined to be ≈92%.[19] After 20 charge/discharge cycles, the Coulombic efficiency was able to reach 98%. These results indicate that the electrochemical Li-storage reversibility is significantly improved by forming a ternary Li_2MgSi compound with respect to that achieved by a binary Mg_2Si compound, which is possibly due to the fact that the formation of metallic Mg during the discharge process is avoided for the Li_2MgSi compound.[15]

Further comparison of the cycle performances of the as-prepared Mg_2Si and hexagonal Li_2MgSi compounds was conducted by plotting the charge capacity as a function of cycle number. The results are shown in Figure 3b. It is clear that the cycling stability of the hexagonal Li_2MgSi is superior to that of the Mg_2Si, especially over the first 30 cycles. The charge capacity of the Mg_2Si was rapidly reduced from 1007 mAh g^{-1}

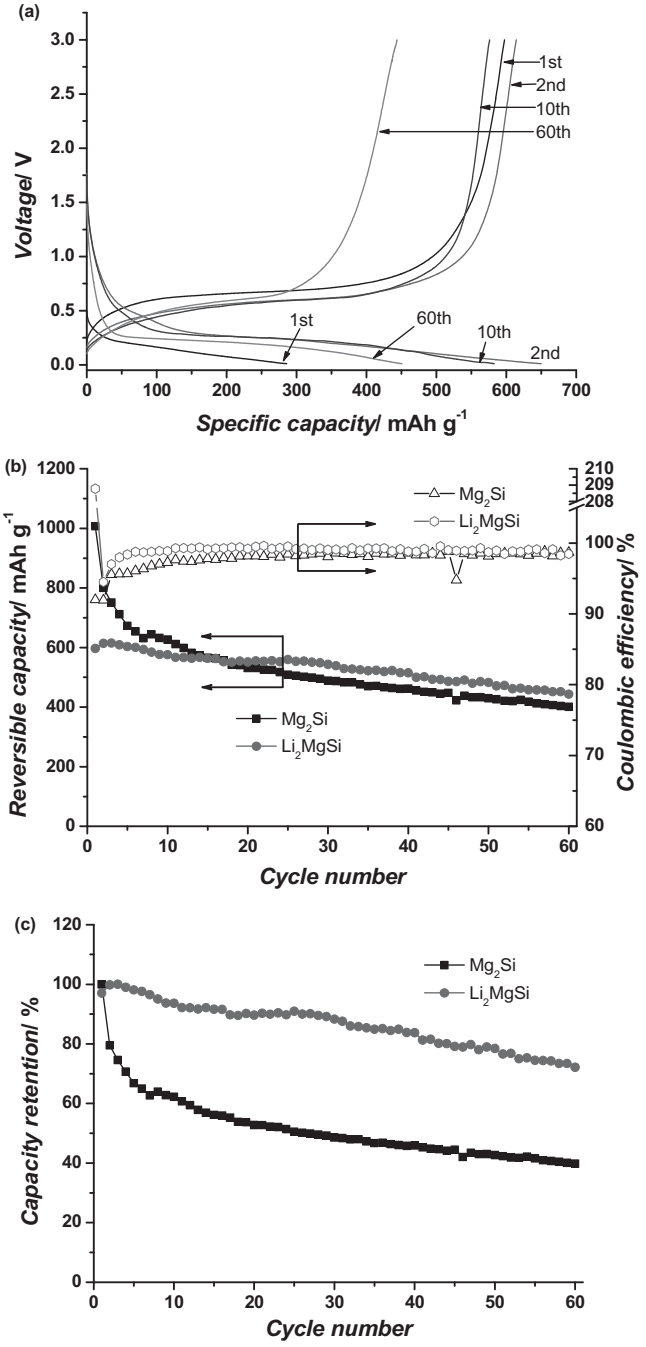

Figure 3. a) Galvanostatic discharge/charge curves of the hexagonal Li_2MgSi anode in the voltage range of 0.01–3.0 V. b) Cycling performance and Coulombic efficiency of Mg_2Si and the hexagonal Li_2MgSi at 100 mA g^{-1} over the voltage range of 0.01–3.0 V. c) Capacity retention of Mg_2Si and the hexagonal Li_2MgSi at 100 mA g^{-1}.

to 489 mAh g^{-1} after 30 charge/discharge cycles and then further decreased to 401 mAh g^{-1} after additional 30 cycles. Such a rapid capacity fading can be attributed to two factors as reported previously.[19] One is the pulverization and disintegration of the electrode with cycling as a large number of cracks and interstices are clearly seen on the surface of electrode after 60 cycles (see Figure S4, Supporting Information), which loses active materials and decreases electrical contact. The other is the irreversible capacity loss caused by the formation of Li–Mg and Li–Si alloys upon lithiation, which is proved by the gradual shortening and even disappearance of voltage plateaus corresponding to the delithiation of Li–Mg and Li–Si alloys upon charging as shown in the galvanostatic cycling voltage profiles (see Figure S5, Supporting Information). Encouragingly, the charge capacity of the Li_2MgSi was first increased from 597 to 615 mAh g^{-1} over the initial three cycles and then gradually decreased to 444 mAh g^{-1} after 60 cycles. By dividing the charge capacity by the maximum charge capacity, the capacity retentions were calculated to be 39.8% and 72.1% for Mg_2Si and Li_2MgSi, respectively, as shown in Figure 3c. Thus, significantly improved cycling stability was achieved for the hexagonal Li_2MgSi relative to the stability of Mg_2Si. It is clear that Li_2MgSi should be a more favorable anode material for Li-ion batteries than Mg_2Si from the perspective of cycling stability.

2.3. Effects of Ball Milling on Li_2MgSi

The theoretical electrochemical capacity of Li_2MgSi as an anode material is calculated to be 808 mAh g^{-1} if all lithium ions in Li_2MgSi are assumed to have been removed. This value is significantly higher than the maximum charge capacity (615 mAh g^{-1}) measured in this case. In addition, the cycling stability of the as-prepared Li_2MgSi must still be further improved because the capacity retention is only 74.3% after 60 cycles. It is well known that particle size has a great impact on the electrochemical properties of the electrode materials for Li-ion batteries. Therefore, ball-milling treatment was further conducted on the as-prepared hexagonal Li_2MgSi to improve its electrochemical performance.

The as-prepared Li_2MgSi was subjected to ball-milling treatment on a planetary ball mill rotating at 500 rpm. The ball-to-sample weight ratio was approximately 30:1. **Figure 4** illustrates the XRD patterns of the Li_2MgSi samples milled for 0–2 h. It is observed that after 0.2 h of ball milling, four new peaks were detected at 24.0°, 31.3°, 47.1° and 57.8° (2θ), although the diffraction peaks of the hexagonal phase still dominate the XRD profile. These four diffraction peaks correspond to the (222), (331), (622), and (800) planes of cubic Li_2MgSi (fluorite-type structure), as reported previously.[21] With increasing ball-milling duration, the diffraction peaks of the hexagonal phase were gradually weakened, and those of the cubic phase increased in relative intensity. When the milling time was extended to 2 h, the diffraction peaks of the hexagonal phase disappeared, and only the reflections of the cubic phase were observed. This result indicates that the hexagonal Li_2MgSi was completely converted to the cubic Li_2MgSi, that is, a polymorphic transformation. In addition, it should be noted that the diffraction peaks were distinctly weakened and broadened after 2 h of ball milling, indicating reduced crystallinity. Thus, energetic ball milling induces a polymorphic transformation of Li_2MgSi from the hexagonal phase to the cubic phase along with a decrease in the crystallinity. We therefore believe that the cubic Li_2MgSi should be metastable with respect to the hexagonal phase. However, a reverse transformation from the cubic phase to the hexagonal phase was not observed while annealing the post-2-h-milled sample at 580 °C for 1 h under 1 bar Ar in addition to the increased crystallinity and the presence of Mg_2Si and Li–Si alloy phases (see Figure S6, Supporting Information). It indicates that the polymorphic transformation caused by ball milling is irreversible.

Figure 5 shows the XRD patterns of Li_2MgSi milled for 2–30 h. As shown, the diffraction peaks were broadened and their intensities were further reduced with increasing ball-milling time, although the pattern remained nearly unchanged, indicating a decrease in the particle/grain size. **Figure 6** displays SEM images of Li_2MgSi milled for 2–30 h. After 2 h of ball milling, the sample showed rather non-uniform particles ranging in size from 0.2 to 1.5 μm. Most of the particles were larger than 1 μm. As the milling time was prolonged from 2 h to 24 h, the particle sizes of the samples gradually decreased and the size distribution became more uniform. After 10 h of ball milling, the particles were nearly spherical in shape and the particle size was 0.4–0.6 μm. The particle size of the post-24-h-milled sample was further reduced to 0.2–0.4 μm. As the milling time was further extended to 30 h, however, the sample

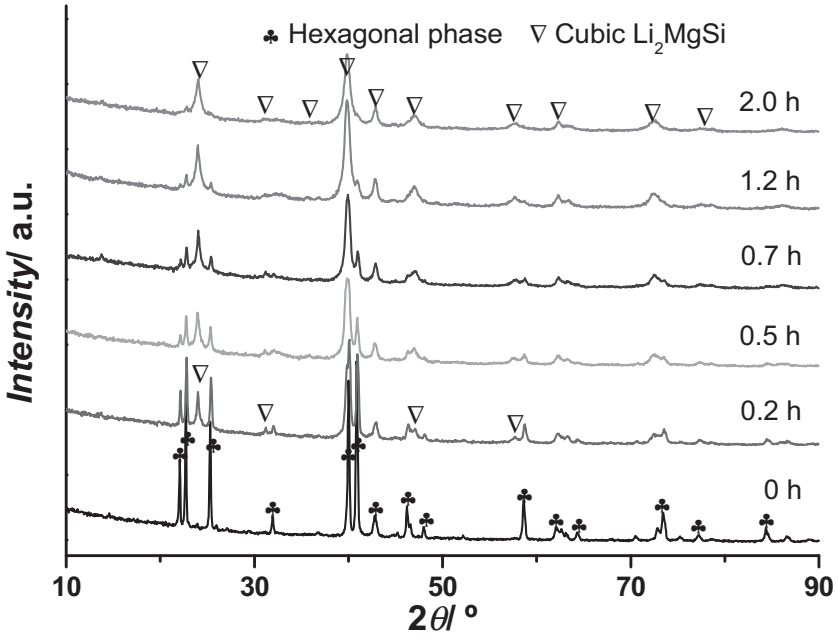

Figure 4. XRD patterns of the Li_2MgSi milled for 0–2 h. ♣: hexagonal phase, ∇: cubic Li_2MgSi.

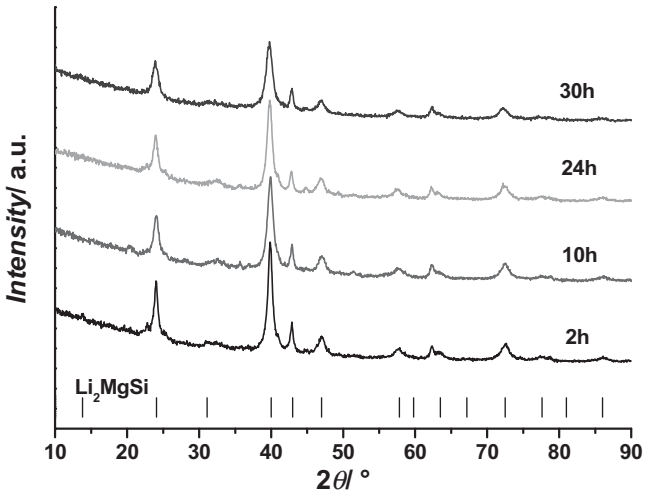

Figure 5. XRD patterns of the Li_2MgSi milled for 2–30 h.

particles became irregular in shape and size along with the aggregation of small particles.

Figure 7a shows the first voltage profiles of the Li_2MgSi milled for different durations. The profiles show a close dependence of the discharge/charge capacities on the milling time. The first discharge/charge capacities for samples milled for different durations first increased and then decreased with milling time. The initial discharge capacities are 210, 254, 355, and 344 mAh g^{-1} for the electrodes milled for 2, 10, 24, and 30 h, respectively, and the corresponding charge capacities are 547, 746, 828, and 781 mAh g^{-1}. Specifically, the appropriate ball-milling treatment significantly reduced the particle and grain sizes of Li_2MgSi, as shown in Figures 5,6. Milling increased the effective specific surface area and reduced the mass transport lengths, consequently increasing the utilization efficiency of the active species and enhancing the discharge/charge capacities.[23] As a result, the optimal milling time is believed to be 24 h in this case.

After the first discharge/charge cycle, the maximum discharge capacity of 808 mAh g^{-1} was achieved for the post-24-h-milled sample, as shown in Figure 7b. In addition, the smallest interval between the discharge and charge plateaus was also observed for the post-24-h-milled Li_2MgSi, reflecting a reduced polarization effect. This finding is closely correlated to the reduced particle size and increased specific surface area, which induced the improved reactivity. It is worth noting that the maximum charge capacity of Li_2MgSi was still slightly lower than that of Mg_2Si even after 24 h of ball milling. This observation can be attributed to two factors. One is that the chemically pre-inserted Li contributed to the molecular weight of Li_2MgSi. The other is that one more mole of Mg in Mg_2Si could be further lithiated to form Li–Mg alloys.

Figure 7c presents the discharge capacity curves of Li_2MgSi milled for different durations as a function of cycle number. It is clear that ball-milling treatment significantly increased the reversible capacity and improved the cycling durability of Li_2MgSi. After 100 cycles, the capacity of the samples milled for 2, 10, 24, and 30 h remained at 275, 342, 405, and 341 mAh g^{-1}, respectively, and the corresponding capacity retentions were calculated to be 43.4%, 43.6%, 50%, and 45% (Figure 7d). The post-24-h-milled Li_2MgSi exhibited the best cycling stability, which should be closely correlated to the improved Coulombic efficiency of the sample. Figure 7d also presents the Coulombic efficiency and capacity retention as a function of milling time. It

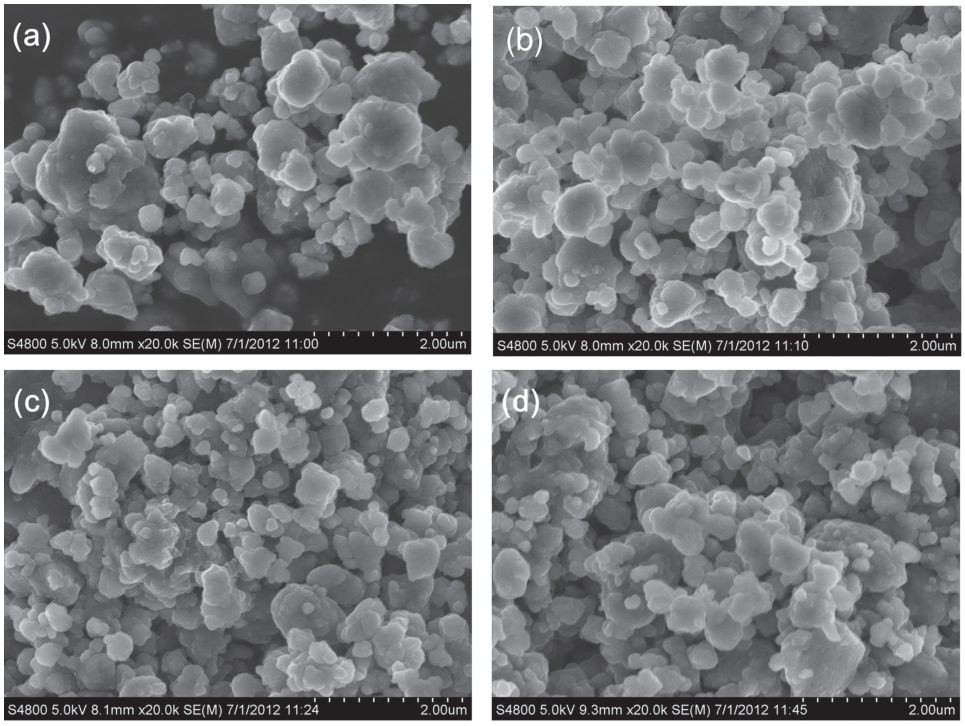

Figure 6. SEM images of the Li_2MgSi milled for a) 2 h, b) 10 h, c) 24 h, and d) 30 h.

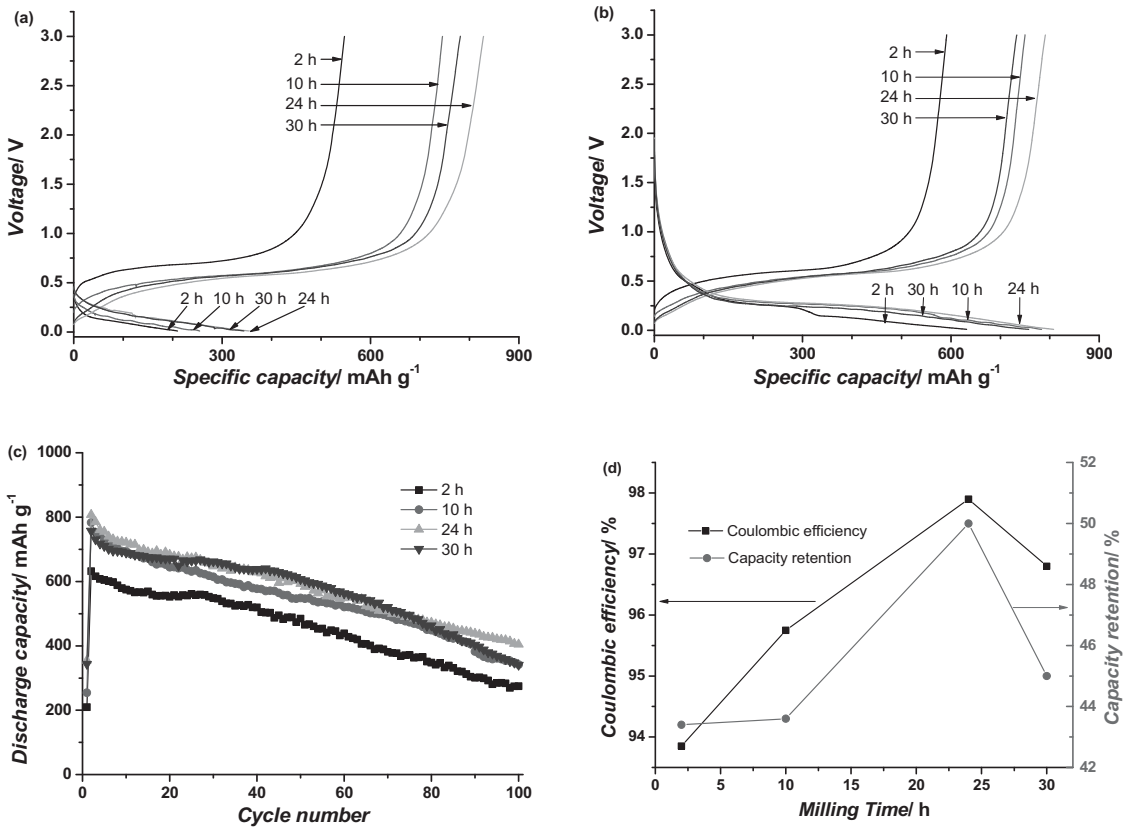

Figure 7. Electrochemical properties of the Li_2MgSi after different milling durations. Voltage profiles of the post-milled Li_2MgSi during a) the first cycle and b) the second cycle. c) Discharge capacity curves as a function of cycle number. d) Coulombic efficiency and capacity retention as a function of milling time.

is observed that with increasing ball milling time, the Coulombic efficiency of the Li_2MgSi electrode during the second cycle first increased and then decreased, and the highest Coulombic efficiency was obtained for the sample milled for 24 h. Interestingly, an identical tendency was observed for the capacity retention after 100 cycles, proving the dependence of the cycling stability on the Coulombic efficiency. Furthermore, the galvanostatic cycling voltage profiles of the post-24-h-milled sample provide additional evidence as the irreversible capacity loss is distinctly decreased with cycling (see Figure S7, Supporting Information). As shown in Figure 6, the post-24-h-milled Li_2MgSi sample exhibited the smallest particle size and the most uniform size distribution in the present study, which should be the most important reason for its improved Li-storage properties. This finding is very helpful in further improving the electrochemical properties of Li_2MgSi as the anodic material for Li-ion batteries. On the other hand, the pre-lithiated Li_2MgSi electrodes may reduce the strain/stress during delithiation/lithiation, which is responsible for the improved cycling stability due to the decreased fracture and pulverization of the electrode (see Figure S4, Supporting Information). Similar phenomenon was also observed in the chemically pre-lithiated $Li_{12}Si_7$ as reported previously.[18]

2.4. Lithium Insertion/Extraction Mechanisms of Li_2MgSi

Cyclic voltammetry (CV) correlated with ex-situ XRD measurement was employed to reveal the lithium insertion/extraction mechanisms of the fluorite-type Li_2MgSi anode. **Figure 8** shows the CV curves of the post-24-h-milled Li_2MgSi anode at the 1st, 2nd, 5th, and 10th cycles. In the first scan, one cathodic peak near 0 V and one anodic peak at 0.75 V were observed, suggesting that only a single-step reduction/oxidation reaction occurred in the first discharge/charge cycle. However, two additional peaks appeared at 0.46 V and 0.17 V in the second scan, indicating that multistep reactions occurred for the lithiation of the active species formed after the first cycle. Interestingly, the newly developed cathodic peak centred at 0.46 V disappeared upon further cycling, and the other remained at approximately 0.17 V in addition to that near 0 V. This phenomenon suggests that an irreversible intermediate may be formed during the second cycle. In addition, the anodic peak was shifted from 0.75 V to 0.6–0.7 V after the first scan, which reduced the potential discrepancy between the anodic and cathodic peaks, indicating improved polarization.

To further understand the lithiation/delithiation mechanism of the Li_2MgSi materials, post-24-h-milled Li_2MgSi electrodes in different lithiation/delithiation states were collected for XRD measurements. **Figure 9** shows the XRD and high-resolution XRD profiles of the samples in different states. The abbreviations "dis" and "char" shown in Figure 9 represent "discharge" and "charge", respectively. To obtain the electrode state at 0.01 V, the as-prepared electrode was first discharged to 0.01 V at 100 mA g^{-1} and then discharged to 0.01 V twice at 10 mA g^{-1} with a 10-min pause between current steps to obtain

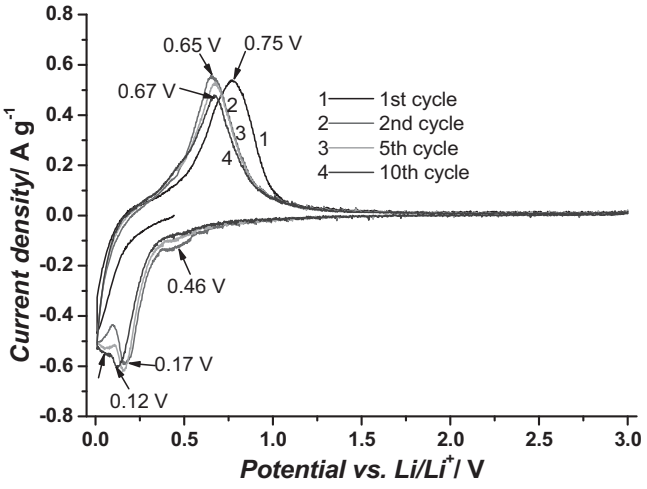

Figure 8. Cyclic voltammetry curves of the post-24-h-milled Li_2MgSi anode at different cycles.

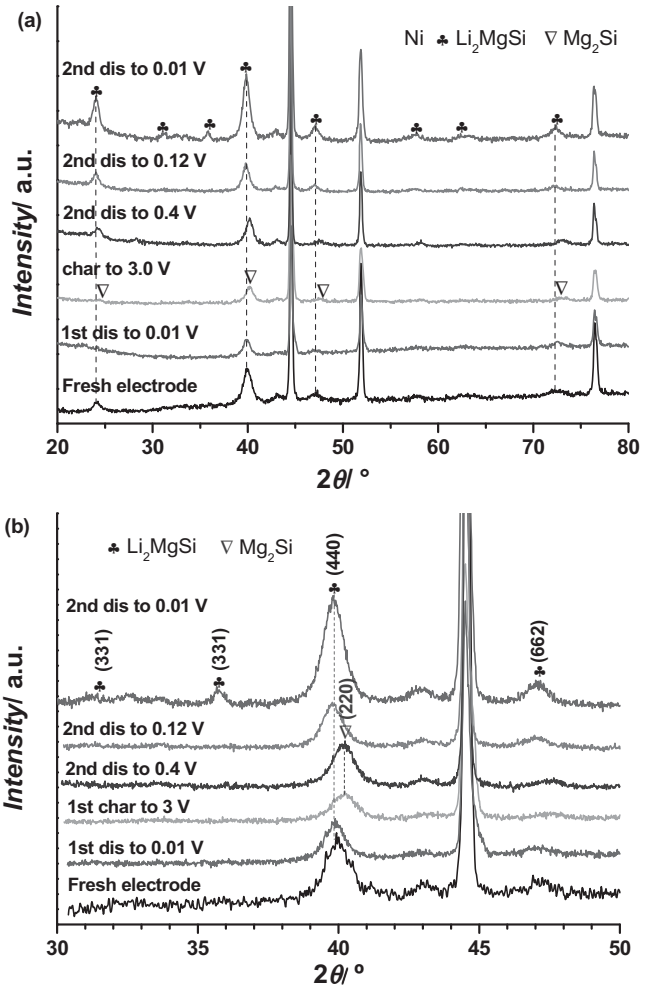

Figure 9. a) XRD and b) high-resolution XRD patterns of the post-24-h-milled Li_2MgSi electrodes in various discharge/charge states. □: Ni, ♣: Li_2MgSi, ∇: Mg_2Si.

a fully lithiated state. The electrode state at 3.0 V was obtained by charging the electrode discharged to 0.01 V in a similar manner. The electrode states at 0.4 and 0.12 V were obtained by discharging the fully charged electrode at 100 mA g^{-1}. It should be mentioned that the diffraction peaks at 44.5°, 51.8° and 76.4° in Figure 9a are attributed to the Ni foam current collectors. The freshly prepared electrode mainly contained the following peaks for the cubic Li_2MgSi structure (space group: $Fm\bar{3}m$): 24.0° for (222), 39.9° for (440), 47.1° for (622), and 72.3° for (844). While discharging to 0.01 V, the relative intensities of the reflections for Li_2MgSi were distinctly weakened. This finding is indicative of the consumption of Li_2MgSi, which can be attributed to the fact that increased lithium insertion led to the conversion of Li_2MgSi to Li-Mg and amorphous Li–Si alloys, as reported previously.[15] However, the characteristic diffraction peaks of Li–Mg alloys were not observed in the XRD profile, as shown in Figure 6, possibly due to the low relative contents of the components.

After the electrode was charged to 3 V, the diffraction peaks at 24.0°, 39.9°, 47.1°, and 72.3° clearly shifted to higher angles. This change was more distinct in the high-resolution XRD profile, as shown in Figure 9b. The reflections are in good agreement with those of Mg_2Si, which has a crystal structure similar to that of Li_2MgSi, though with a slightly smaller unit cell.[22] That is, Mg_2Si was formed after the specimen was charged to 3.0 V. Because the formation of Mg_2Si consumes only half of the Si atoms in Li_2MgSi, it was hypothesized that the amorphous Li_xSi/Si should also be involved in the delithiation process. Therefore, the delithiation reaction of Li_2MgSi is proposed to occur as follows:

$$Li_2MgSi \rightarrow Mg_2Si + Li_xSi/Si + Li^+ + e^- \quad (2)$$

This reaction corresponds to the anodic peak at 0.6–0.8 V in the CV curves. It should be mentioned that the Li_xSi/Si formed during the delithiation process of Li_2MgSi may be amorphous because crystalline Si readily becomes amorphous form after a single discharge/charge cycle,[24] which is responsible for its invisibility in the XRD profile.

For the electrode discharged to 0.4 V, no distinct change in the XRD profile was observed with respect to that charged to 3.0 V. This result suggests that lithium insertion into Mg_2Si did not occur during this process because no Li_2MgSi was detected. In previous reports, the lithiation of Li–Si alloy occurred above 0.4 V during lithium insertion into Mg_2Si.[13,15] We therefore speculate that the cathodic peak at 0.46 V shown in Figure 8 can be attributed to the further lithiation of the Li–Si alloy that was extracted from Li_2MgSi during the first lithiation. It is known that Si-based anodic materials undergo a large volume change during charge/discharge.[25] This change in volume leads to severe electrode pulverization and subsequent electrical disconnection from current collectors, which is the main reason for the gradual weakening and even absence of the cathodic peak at 0.46 V during subsequent cycling.

While further discharging to 0.12 V, a low-angle shift was observed for the diffraction peaks of the resulting product in the XRD pattern, implying an expansion of the unit cell. Further high-resolution results revealed that the peak at 40.2° for the (220) plane of Mg_2Si shifted to 39.9°, as shown in Figure 9b.

It is well known that during the lithiation process of Mg_2Si, the formation of either Li_xMg_2Si or Li_2MgSi can result in the expansion of the unit cell. However, the absence of the characteristic peaks of Li_2MgSi at 31.3° and 36.1° suggests that the low-angle shift of the reflections is mainly attributed to the formation of Li_xMg_2Si. Therefore, the cathodic peak at 0.12–0.17 V in the CV curves was mainly attributed to lithium insertion into Mg_2Si to form Li_xMg_2Si, as described by the following reaction:

$$Mg_2Si + yLi^+ + ye^- \rightarrow Li_yMg_2Si\ (0 < y \leq 1) \quad (3)$$

After the electrode was discharged to 0.01 V again, the intensities of the diffraction peaks were distinctly enhanced, and two peaks at 31.3° and 36.1° were also discernible, although their intensities were quite weak. This observation unambiguously indicates the formation of Li_2MgSi because no reflections for Mg_2Si occurred in the vicinity of these peaks. Moreover, no peaks in addition to those of the Ni foam were observed in the XRD profile. Specifically, the increased intensities of the diffraction peaks indicate improved crystallinity. Thus, we believe that the electrochemical reaction that occurred near 0 V can be expressed as follows:

$$Li_xSi/Si + Li_yMg_2Si + Li^+ + e^- \rightarrow Li_2MgSi \quad (4)$$

According to this reaction, it is clear that Li_xSi/Si and Li_yMg_2Si together react with Li to produce Li_2MgSi, which prevents the capacity fading caused by the dissociation of Mg from Li_yMg_2Si and the pulverization of Li_xSi/Si during lithiation.

According to the above discussion, we provide a description of the detailed electrochemical events that occurred during the discharge/charge process of the Li_2MgSi anode. First, a small portion of the Li_2MgSi was converted to Li–Si or Li–Mg alloys as the electrode was discharged to 0.01 V. Then, Mg_2Si and amorphous Li_xSi/Si were formed after the electrode was charged to 3.0 V. During the subsequent discharge process, the further lithiation of Li–Si alloy first occurred at 0.55–0.37 V. Mg_2Si was then lithiated to form Li_xMg_2Si at 0.37–0.08 V. Lastly, Li_2MgSi was formed again when the electrode was discharged to 0.01 V. It is noteworthy that the dissociation of Mg or Li–Mg alloys during the lithium insertion into Mg_2Si was not observed. We therefore believe that the formation of metallic Mg was effectively avoided during the discharge/charge process of the Li_2MgSi anode, which is one of the most important reasons for the improved cycling stability of the Li_2MgSi electrode compared with that of the Mg_2Si electrode.

3. Conclusions

A new single hexagonal Li_2MgSi phase was synthesized by a hydrogen-driven chemical reaction at 580 °C. The as-prepared Li_2MgSi compound exhibited improved cycling stability as an anode material of Li-ion batteries with respect to the cycling stability of Mg_2Si. The capacity retention of the Li_2MgSi anode was nearly twice that of Mg_2Si after 60 cycles. Examinations of ball-milled specimens revealed that a polymorphic transformation of Li_2MgSi occurred from the hexagonal phase to the cubic phase after 2 h of milling. Further ball-milling treatment increased the maximum discharge/charge capacities and improved the cycling stability of the fluorite-type Li_2MgSi. The sample milled for 24 h exhibited optimized capacity, Coulombic efficiency and capacity retention. The maximum discharge capacity of the post-24-h-milled Li_2MgSi anode was 828 mAh g^{-1}, and the capacity retention of the anode was 50% after 100 cycles. SEM observations sample indicated that the particle size decreased and the size distribution improved for the post-24-h-milled sample. Ex-situ XRD results correlated with CV examinations revealed that the dissociation of metallic Mg and/or Li–Mg alloy from Mg_2Si during the lithiation process was effectively avoided, which consequently contributed to the improved cycling stability of the Li_2MgSi electrode. The findings presented in this work provide guidelines for the design and synthesis of new Si-based anode materials with favorable electrochemical properties for Li-ion batteries.

4. Experimental Section

Materials and Synthesis: LiH (purity 98%, Alfa Aesar), silicon (purity 99.9%, Shanghai ST-NANO) and MgH_2 (purity 98%, Alfa Aesar) were purchased and used as received. A mixture of LiH, MgH_2, and Si in a molar ratio of 2:1:1 (donated as 2LiH-MgH_2-Si) was first ball milled on a planetary ball mill (QM-1SP4, Nanjing) at 300 rpm for 4 h under an argon atmosphere. The ball-to-sample weight ratio was approximately 40:1. Temperature-programmed desorption measurements (TPD) were conducted on a homemade instrument equipped with an online gas chromatograph (GC) for the rapid scanning of the gas desorption behavior upon heating, and an appropriate temperature range for volumetric release was then determined. Sample (≈40 mg) was loaded and tested. Pure Ar was used as the carrier gas, and the temperature was elevated at 5 °C min^{-1}. All handling of samples was carried out under anaerobic (O_2: <0.1 ppm) and anhydrous (H_2O: <0.1 ppm) conditions inside a MBRAUN glovebox filled with pure argon to prevent the materials from being contaminated by air and moisture.

The quantitative dehydrogenation behavior of the 2LiH-MgH_2-Si mixture was evaluated by a volumetric method. In a typical procedure, sample (≈1.5 g) was first loaded into a stainless steel tube reactor in a glovebox. The reactor was then connected to a Sieverts-type apparatus. After evacuating the reactor and the system to a primary vacuum (10^{-3} bar) at room temperature, the sample was gradually heated to 560–600 °C at a rate of 5 °C min^{-1} for chemical reaction and hydrogen release. The amount of hydrogen released was calculated from the pressure change measured in the calibrated volume using the equation of state.

Characterization: Structural identification was performed on a PANalytical X'Pert Pro X-ray Diffractometer (XRD) with Cu-Kα radiation at 40 kV and 40 mA. XRD data were collected over the 2θ range of 10° to 90° in increments of 0.05°. High-resolution XRD data were acquired over the 2θ range of 30° to 50° in increments of 0.016°. Cycled electrodes were washed with anhydrous diethyl carbonate (DEC) to remove the remaining electrolyte before XRD measurements. A specially designed container was used to protect samples from being contaminated by air and moisture.

The morphology of the alloys was observed by a scanning electron microscope (SEM, Hitachi-SU70, Japan). Pure nitrogen was used to protect the samples from contamination of air and moisture during their transfer from the glovebox to the SEM facility. An energy-dispersive X-ray spectrometer (EDS) was employed to analyze the chemical composition of the samples.

Electrochemical Measurements: The working electrode was prepared by ball milling the active materials with acetylene black in a weight ratio of 3:1 for 3 h. The ball-to-sample weight ratio was 150:1. The resulting powder (≈5 mg) was then uniformly spread onto a nickel foam current collector with an area of 1.33 cm^2. Next, the electrode was cold-pressed

under a pressure of approximately 10 MPa. The half-cells (2025 coin-type cells) were assembled in an argon-filled glovebox with lithium metal as the counter electrode and reference electrode. A solution of 1 M $LiPF_6$ with ethylene carbonate (EC)/dimethyl carbonate (DMC) (1:1 by volume) was used as the electrolyte.

The cells were discharged under a constant current density of 100 mA g^{-1} from an initial open-circuit potential to 0.01 V (vs Li/Li^+) to prevent possible lithium deposition on the electrode and then cycled galvanostatically over a voltage range of 0.01–3.0 V using a Neware battery test system (Shenzhen, China). Cyclic voltammograms (CVs) of the cells were measured on an Arbin potentiostat (BT-2000, USA) at a scan rate of 0.1 mV s^{-1} over a potential range of 0.01–3.0 V. Lithium insertion and extraction in electrode were referred to as discharge and charge, respectively.

Supporting Information

Supporting Information is available from the Wiley Online Library or from the author.

Acknowledgements

The authors gratefully acknowledge the financial support received from the National Nature Science Foundation of China (51025102, 51171170 and 51222101), the Research Fund for the Doctoral Program of Higher Education of China (20130101110080 and 20130101130007), the Program for Innovative Research Team in University of Ministry of Education of China (IRT13037), and the Fundamental Research Funds for the Central Universities (2014XZZX003-008).

Received: December 26, 2013
Revised: February 8, 2014
Published online: March 24, 2014

[1] B. L. Ellis, K. T. Lee, L. F. Nazar, *Chem. Mater.* **2010**, *22*, 691.
[2] A. S. Aricò, P. Bruce, B. Scrosati, J. Tarascon, W. Van Schalkwijk, *Nat. Mater.* **2005**, *4*, 366.
[3] M. Wagemaker, F. M. Mulder, *Acc. Chem. Res.* **2012**, *46*, 1206.
[4] W. Tang, Y. Zhu, Y. Hou, L. Liu, Y. Wu, K. P. Loh, H. Zhang, K. Zhu, *Energy Environ. Sci.* **2013**, *6*, 2093.
[5] R. Fong, U. Vonsacken, J. R. Dahn, *J. Electrochem. Soc.* **1990**, *137*, 2009.
[6] M. Ebner, F. Marone, M. Stampanoni, V. Wood, *Science* **2013**, *342*, 716.
[7] Y. Gu, F. Wu, Y. Wang, *Adv. Funct. Mater.* **2013**, *23*, 893.
[8] A. Mahmoud, M. Chamas, J. Jumas, B. Philippe, R. Dedryvère, D. Gonbeau, I. Saadoune, P. Lippens, *J. Power Sources* **2013**, *244*, 246.
[9] M. Zeilinger, V. Baran, L. van Wüllen, U. Häussermann, T. F. Fässler, *Chem. Mater.* **2013**, *25*, 4113.
[10] C. M. Park, J. H. Kim, H. Kim, H. J. Sohn, *Chem. Soc. Rev.* **2010**, *39*, 3115.
[11] J. O. Besenhard, J. Yang, M. Winter, *J. Power Sources* **1997**, *68*, 87.
[12] J. M. Yan, H. Z. Huang, J. Zhang, Y. Yang, *J. Power Sources* **2008**, *175*, 547.
[13] H. Kim, J. Choi, H. J. Sohn, T. Kang, *J. Electrochem. Soc.* **1999**, *146*, 4401.
[14] S. Song, K. A. Striebel, R. P. Reade, G. A. Roberts, E. J. Cairns, *J. Electrochem. Soc.* **2003**, *150*, A121.
[15] G. A. Roberts, E. J. Cairns, J. A. Reimer, *J. Electrochem. Soc.* **2004**, *151*, A493.
[16] G. A. Roberts, E. J. Cairns, J. A. Reimer, *J. Power Sources* **2002**, *110*, 424.
[17] Y. Imai, A. Watanabe, *J. Alloys Compd.* **2011**, *509*, 7877.
[18] R. J. Ma, Y. F. Liu, Y. P. He, M. X. Gao, H. G. Pan, *J. Phys. Chem. Lett.* **2012**, *3*, 3555.
[19] Y. F. Liu, Y. P. He, R. J. Ma, M. X. Gao, H. G. Pan, *Electrochem. Commun.* **2012**, *25*, 15.
[20] J. F. Herbst, M. S. Meyer, *J. Alloys Compd.* **2010**, *492*, 65.
[21] T. Moriga, K. Watanabe, D. Tsuji, S. Massaki, I. Nakabayashi, *J. Solid State Chem.* **2000**, *153*, 386.
[22] S. Wengert, R. Nesper, W. Andreoni, M. Parrinello, *Phys. Rev. Lett.* **1996**, *77*, 5083.
[23] R. Pitchai, V. Thavasi, S. G. Mhaisalkar, S. Ramakrishna, *J. Mater. Chem.* **2011**, *21*, 11040.
[24] P. Limthongkul, Y. I. Jang, N. J. Dudney, Y. M. Chiang, *Acta Mater.* **2003**, *51*, 1103.
[25] M. N. Obrovac, L. J. Krause, *J. Electrochem. Soc.* **2007**, *154*, A103.